Role of large-scale velocity fluctuations in a two-vortex kinematic dynamo

E. J. Kaplan,[1,2,*] B. P. Brown,[1,2] K. Rahbarnia,[1,2] and C. B. Forest[1,2]

[1]*Department of Physics, University of Wisconsin–Madison, 1150 University Avenue, Madison, Wisconsin 53706, USA*

[2]*Center for Magnetic-Self Organization in Laboratory and Astrophysical Plasmas, University of Wisconsin–Madison, 21 North Park Street, Madison, Wisconsin 53715, USA*

(Received 10 April 2012; revised manuscript received 24 May 2012; published 20 June 2012)

This paper presents an analysis of the Dudley-James two-vortex flow, which inspired several laboratory-scale liquid-metal experiments, in order to better demonstrate its relation to astrophysical dynamos. A coordinate transformation splits the flow into components that are axisymmetric and nonaxisymmetric relative to the induced magnetic dipole moment. The reformulation gives the flow the same dynamo ingredients as are present in more complicated convection-driven dynamo simulations. These ingredients are currents driven by the mean flow and currents driven by correlations between fluctuations in the flow and fluctuations in the magnetic field. The simple model allows us to isolate the dynamics of the growing eigenvector and trace them back to individual three-wave couplings between the magnetic field and the flow. This simple model demonstrates the necessity of poloidal advection in sustaining the dynamo and points to the effect of large-scale flow fluctuations in exciting a dynamo magnetic field.

DOI: 10.1103/PhysRevE.85.066315 PACS number(s): 47.27.er, 95.30.Qd, 91.25.Cw, 96.60.Hv

I. INTRODUCTION

Long has it been known that the magnetic fields of astrophysical objects are generated by flows of conductive media within their interiors [1] and significant investments have been made in both theory (with three-dimensional codes running on modern supercomputers [2–4]) and laboratory experiments [5,6] to capture the dynamics of the magnetic and velocity fields. Large-scale flow shear contributes to the formation of axisymmetric magnetic fields, but Cowling's antidynamo theorem dictates that no axisymmetric flow of a conductive medium can excite an axisymmetric magnetic field [7]. Instead, fluctuating, nonaxisymmetric flows and fields must coherently interact to close the axisymmetric dynamo loop. Laboratory dynamo experiments in Refs. [5,6] are designed around simple, axisymmetric, two-vortex flows that can, at least theoretically, excite nonaxisymmetric dipole magnetic fields. Many stellar dynamo simulations achieve complicated convective flows with no assumed axisymmetry that excite axisymmetric dipole fields. These simulations build up a magnetic field out of toroidal shear, advection, diffusion, and electric currents induced by helical eddies in the conductive medium.

In stars and planets the natural axis of symmetry is the rotation axis, as the rotation of the system is typically much faster than the flows of the conducting fluid (plasma in stars and iron in planets). As a result, the flows are rotationally constrained. Observations of dynamo-generated magnetic fields in the Sun, Earth, and various planetary bodies (e.g., Saturn, Jupiter, and some moons) generally indicate a highly axisymmetric field though there are some exceptions (e.g., Uranus and Neptune) [8]. In simulations of stellar dynamos (e.g., Refs. [2–4,9,10]) convection establishes highly complex nonaxisymmetric flows as well as large-scale axisymmetric flows with differential rotation that act together to generate strong global-scale axisymmetric fields. Latitudinal and radial shear in the differential rotation amplifies axisymmetric toroidal fields, while the axisymmetric poloidal (dipolelike) field is generated by turbulent correlations between the fluctuating nonaxisymmetric flows and fields. At present it is unclear whether these correlated fluctuations are due to large-scale flows or due to small-scale helical eddies in the conductive medium. Here, in the context of laboratory flows, we will study a system where the former yield an axisymmetric poloidal field.

The typical framework for describing the dynamo effect relies upon mean-field theory [11], where small-scale fluctuations in the magnetic field and in the flow of the medium coherently interact and generate a large-scale magnetic field. Mean-field theory is built upon the assumption of isotropic turbulence and a separation of scales between the flow of the conductor and the induced magnetic field. Much of the discussion of mean-field effects focuses on these scale-separated eddies [3,12], but there is numerical [13,14] and experimental [5] evidence that the large eddies are essential to understanding the conditions for dynamo onset.

This discussion will take a simple flow, the two-vortex ($t2s2$) flow of Dudley and James [15], and analyze the specific dynamic effects that allow it to excite a magnetic field. This flow is chosen because of its similarity to the von Kármán and Taylor-Green flows. It is probably the simplest possible flow that generates a steady, dipolar magnetic field and forms the basis for a large amount of numerical [16] and experimental work [5,17]. Figure 1 shows a three-dimensional visualization of the flow and its dipolar eigenmode. A coordinate rotation converts the flow and the magnetic eigenmode from purely axisymmetric flow and purely nonaxisymmetric field definitions to combinations of axisymmetric and nonaxisymmetric components for both and thus opens up the dynamo system to a mean-field analysis.

The rest of this paper will proceed as follows. Section II will describe the kinematic dynamo problem. Section III will describe the coordinate transformation between axisymmetric flows and axisymmetric magnetic fields and define the mean-flow-driven and fluctuation-driven emfs. Section IV will relate

*ejkaplan@wisc.edu

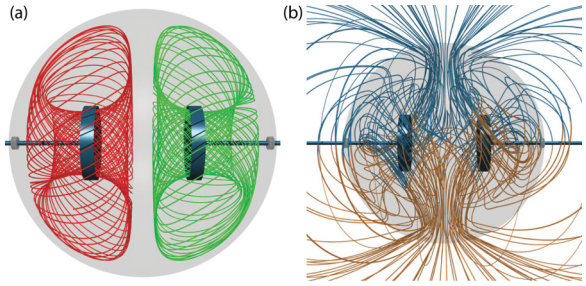

FIG. 1. (Color online) VAPOR [18] rendering of (a) the Dudley-James two-vortex flow and (b) the transverse dipole eigenmode that it excites. Reprinted from Ref. [16].

the fluctuation-driven emfs found in the Dudley-James two-vortex flow to the fluctuation-driven emfs of mean-field theory. Section V will explore the role of pitch angle and mean flow in exciting a dynamo from the $t2s2$ flow. Section VI summarizes the paper.

II. KINEMATIC DYNAMO MODEL

A typical first step in designing an experiment (numerical or physical) is to solve the corresponding kinematic dynamo problem, where the flow of the conductor is considered fixed and only the magnetic induction equation

$$\frac{\partial \mathbf{B}}{\partial \tau} = \mathrm{Rm}\nabla \times (\mathbf{v} \times \mathbf{B}) + \nabla^2 \mathbf{B} \tag{1}$$

is considered. Here $\mathbf{v}$ is the (normalized) velocity field; $\mathbf{B}$ is the magnetic field; $\mathrm{Rm} = v_0 a/\eta$ is the magnetic Reynolds number, with v_0, a, and η the characteristic velocity, length, and magnetic diffusivity of the medium, respectively; and $\tau = t\eta/a^2$ is the time normalized by the diffusion time. The usual treatment of the problem in spherical geometries is to convert from the spatial domain to a spectral domain by decomposing the magnetic fields and flows into vector spherical harmonics represented as

$$\begin{aligned}\mathbf{B}(r,\theta,\phi) &= \sum_i \nabla \times \nabla \times S_{\ell_i}^{m_i}(r) Y_{\ell_i}^{m_i}(\theta,\phi)\mathbf{e}_r \\ &\quad + \nabla \times T_{\ell_i}^{m_i}(r) Y_{\ell_i}^{m_i}(\theta,\phi)\mathbf{e}_r, \\ &= \sum_i \frac{S_{\ell_i}^{m_i}\ell_i(\ell_i+1)Y_{\ell_i}^{m_i}}{r^2}\mathbf{e}_r \\ &\quad + \left(\frac{1}{r}\frac{dS_{\ell_i}^{m_i}}{dr}\frac{\partial Y_{\ell_i}^{m_i}}{\partial\theta} + \frac{T_{\ell_i}^{m_i}}{r\sin(\theta)}\frac{\partial Y_{\ell_i}^{m_i}}{\partial\phi}\right)\mathbf{e}_\theta \\ &\quad + \left(\frac{1}{r\sin(\theta)}\frac{dS_{\ell_i}^{m_i}}{dr}\frac{\partial Y_{\ell_i}^{m_i}}{\partial\phi} - \frac{T_{\ell_i}^{m_i}}{r}\frac{\partial Y_{\ell_i}^{m_i}}{\partial\theta}\right)\mathbf{e}_\phi. \end{aligned} \tag{2}$$

Here S and T represent poloidal and toroidal harmonics respectively, $\mathbf{e}_{r,\theta,\phi}$ are the unit vectors, and the $Y_{\ell_i}^{m_i}(\theta,\phi)$ are (real, unnormalized) spherical harmonics (defined in Appendix A). The azimuthal phase of the harmonic is indicated by $Y_\ell^{m\,c(s)}$, where c and s represent cosine and sine. Harmonics with $m_i = 0$ have no derivative in the azimuthal direction ($\partial_\phi Y_{\ell_i}^0 = 0$). Flows are represented the same way, but with lower case s and t. In general, boldface $\mathbf{B}$ and $\mathbf{v}$ indicate the full spatial vector fields and italic B_i and v_i indicate a single (arbitrary) spectral harmonics.

There is a set of selection rules for describing the $\mathbf{v} \times \mathbf{b}$ interactions of flows with magnetic fields akin to the selection rules of energy level transitions in quantum mechanics. It is based upon the Gaunt K and Elsasser L integrals with

$$K_{ijk} = \int_0^\pi \sin(\theta)d\theta \int_0^{2\pi} d\phi\, Y_i(\theta,\phi)Y_j(\theta,\phi)Y_k(\theta,\phi), \tag{3}$$

$$L_{ijk} = \int_0^\pi d\theta \int_0^{2\pi} d\phi\, Y_i(\theta,\phi)\left(\frac{dY_j(\theta,\phi)}{d\theta}\frac{dY_k(\theta,\phi)}{d\phi} - \frac{dY_j(\theta,\phi)}{d\phi}\frac{dY_k(\theta,\phi)}{d\theta}\right), \tag{4}$$

respectively, where we note that $L_{jik} = -L_{ijk}$.

In the spectral domain, Eq. (1) is composed of a diffusion operator D,

$$D = \sum_k \frac{\partial^2 B_k}{\partial r^2} - \frac{\ell_k(\ell_k+1)}{r^2}B_k, \tag{5}$$

and a flow operator F based on mode-mode interactions,

$$F = \sum_{i,j,k} B_j \overset{v_i}{\to} B_k, \tag{6}$$

where $B_j \overset{v_i}{\to} B_k$ represents the conversion of the magnetic harmonic B_j by the flow harmonic v_i into the magnetic harmonic B_k (see Appendix A for the definition of these interactions). The selection rules of Eqs. (3) and (4) greatly simplify the calculation of F. Interactions of the form $S \overset{s}{\to} S$, $T \overset{s}{\to} T$, and $S \overset{t}{\to} T$ include Gaunt integrals [Eq. (3)], while interactions of the form $T \overset{s}{\to} S$, $S \overset{s}{\to} T$, $S \overset{t}{\to} S$, and $T \overset{t}{\to} T$ include Elsasser integrals [Eq. (4)]. Interactions of the form $T \overset{t}{\to} S$ are identically zero. We seek eigenvector solutions of the magnetic induction equation

$$\lambda\vec{\mathbf{b}} = (\mathrm{Rm}F + D)\vec{\mathbf{b}}. \tag{7}$$

Here λ represents the exponential growth or decay rate of the eigenfunction $\vec{\mathbf{b}}$. Useful quantities to consider will be the amount of energy in a given magnetic harmonic over the spherical domain, represented by $\langle B_k|B_k\rangle$, and the strength of a given interaction of three harmonics over the spherical domain, represented by $\langle B_j|v_i|B_k\rangle$ (see Appendix A for their exact definitions).

Kinematic dynamo studies generally focus on the onset conditions for a growing eigenmode (both in the magnetic Reynolds number and in the specific flow geometry) or the structure of the induced magnetic field [19]. Here we consider both for the two-vortex ($t2s2$) flow of Dudley and James [15]:

$$v = s_2^0(r) + t_2^0(r), \tag{8}$$

where

$$s_2^0(r) = \epsilon r^2 \sin(\pi r),$$
$$t_2^0(r) = r^2 \sin(\pi r),$$

which is known to be dynamo unstable at comparatively small Rm. The factor ϵ represents the pitch of the flow s/t and is set to 0.14 for most of the discussion here.

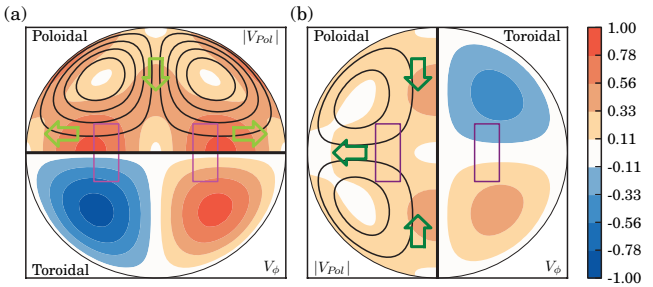

FIG. 2. (Color online) Mean components of the two vortex flow about (a) the flow and (b) magnetic field symmetry axes. The thin black lines represent poloidal streamlines, the thick black lines represent the symmetry axes, the arrows indicate the direction of the mean poloidal flow, and the rectangles indicate the location of impellers that might drive such a flow (as in the experiment in Ref. [5]).

III. COORDINATE TRANSFORM

The Dudley-James two-vortex flow generates a nonaxisymmetric field from an axisymmetric flow, as is necessary under Cowling's theorem [7]. In laboratory settings, it has been natural to define the axis of symmetry by the driving apparatus [the horizontal axis defined by the impellers in Fig. 1(a)], in which case the Dudley-James flow is axisymmetric. However, a sphere has no natural axis of symmetry unless one is set by the properties of the problem being solved. One could instead consider the generated magnetic field to include an axisymmetric field and define the spherical coordinates relative to that axis [the vertical axis defined by the dipole field in Fig. 1(b)]. This is a natural choice, as stellar and planetary dynamo-generated fields tend to have strong axisymmetric components aligned with the stellar or planetary rotation axis. This transformation is necessary to apply a mean-field formulation of the dynamo problem. Without the transformation we have axisymmetric flows acting on azimuthally fluctuating magnetic fields and there is no mean (axisymmetric) field. In the coordinate system presented herein we have azimuthally fluctuating flows interacting with azimuthally fluctuating magnetic fields to generate an axisymmetric magnetic field.

The transformation from spherical harmonics defined about one axis to another comes from the calculation of Wigner D functions [20]. In the case where a transverse dipole Y_1^{1c} becomes an axisymmetric dipole Y_1^0, the second axisymmetric spherical harmonic transforms as

$$Y_2^0(\theta,\phi) = -\tfrac{1}{2}Y_2^0(\theta',\phi') + \tfrac{1}{4}Y_2^{2c}(\theta',\phi'), \qquad (9)$$

i.e., the flow now has both axisymmetric and nonaxisymmetric components relative to the induced axisymmetric dipole field. We term the axisymmetric fields and flows as mean and the nonaxisymmetric fields and flows as fluctuations. Figure 2 shows the change in the mean flows from the change in coordinates. The advantage of a spherical geometry over a cylindrical geometry is that this transformation is easy to perform and requires no change to the machinery of the eigenmode calculation.

The two-vortex flow implies a dynamo cycle where a toroidal flow creates a toroidal field from a poloidal field and then the helical flow converts the toroidal field back into

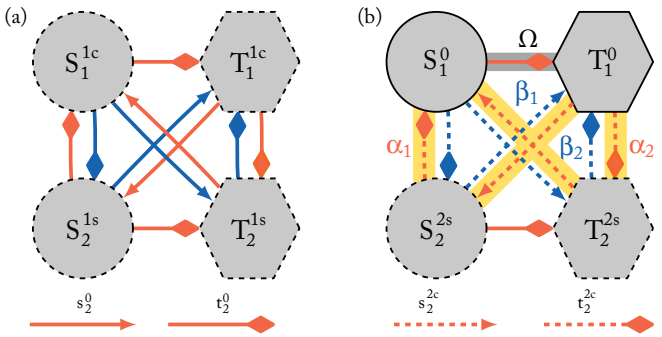

FIG. 3. (Color online) Network diagram of the largest-scale magnetic fields generated by a Dudley-James two-vortex (t_2^0,s_2^0) dynamo in both the (a) axisymmetric flow and (b) mean-field configurations. Each node represents a magnetic field harmonic and each edge (arrow that connects two nodes) represents a flow (the legend is along the bottom). Orange (light) arrows indicate that the energy in the target harmonic is being increased and blue (dark) arrows indicate that the energy in the target harmonic is being decreased. In the mean-field configuration the Ω effect is highlighted and labeled, the possible pathways for the α effect are also highlighted and labeled, and the β effect that removes energy from the mean toroidal field [according to Eq. (4)] is labeled. Solid lines in the borders of the nodes and in the edges indicate an aximuthally symmetric mode. Dashed lines indicate an azimuthal fluctuation.

the poloidal field, thus closing the dynamo cycle. Figure 3 shows a simplified network representation of this cycle in both an axisymmetric flow system [Fig. 3(a)] and a mean-field system [Fig. 3(b)] representation. These figures represent the same process in different coordinate systems, so we shall describe only the mean-field representation [Fig. 3(b)]. Here an existing axisymmetric poloidal dipole field S_1^0 is stretched into an axisymmetric toroidal magnetic field T_1^0 by differential rotation (the t_2^0 flow harmonic, labeled Ω in the figure). This toroidal field is then converted into a fluctuating poloidal magnetic field S_2^{2s} by a fluctuating poloidal flow s_2^{2c}. This fluctuating poloidal field interacts with the fluctuating poloidal flow to remove energy from the axisymmetric toroidal field (interaction β_1 in the network). The fluctuating poloidal field also interacts with the fluctuating toroidal flow t_2^{2c} and by this interaction is converted back into the original poloidal dipole. This entire process is highlighted and labeled as α_1 in the network. Similarly the axisymmetric toroidal field T_1^0 is converted by the fluctuating toroidal flow into a fluctuating toroidal magnetic field, which then interacts with the fluctuating poloidal flow to be converted back into the axisymmetric dipole field (labeled as β_2 and α_2 in the network). The conversion of one magnetic harmonic into another by a given flow is indicated by matched blue (dark) and orange (light) arrows. The orange (light) arrows indicate the increase of the destination harmonic, while the blue (dark) arrows indicate the decrease of the source harmonic. These same processes are present in the axisymmetric flow system [Fig. 3(a)], but there is no way to disentangle the mean Ω and fluctuating α and β effects.

These networks are made by considering only the selection rules [Eqs. (3) and (4)]. Each node in the network represents a magnetic field harmonic and each edge (an arrow that connect

two nodes) represents a valid interaction $B_j \xrightarrow{v_i} B_k$ [as in Eq. (6)]. For example, in the $S_1^0 \xrightarrow{t_2^0} T_1^0$ interaction the t_2^0 flow acts on the S_1^0 to increases the energy in the T_1^0 harmonic.

We now turn to consider the interactions mediated by fluctuating flows and field. The $T_1^0 \xrightarrow{s_2^{2c}} S_2^{2s}$ and the $S_2^{2s} \xrightarrow{s_2^{2c}} T_1^0$ interactions involve the same harmonics with the j and k indices interchanged. As these interactions have the Elsasser integral as a factor, the interchange of indices flips the sign of the interaction. Therefore, if $T_1^0 \xrightarrow{s_2^{2c}} S_2^{2s}$ is increasing the energy in the S_2^{2s} harmonic, $S_2^{2s} \xrightarrow{s_2^{2c}} T_1^0$ is simultaneously decreasing the energy in the T_1^0 harmonic and energy flows from T_1^0 to S_2^{2s}. This representation is a natural analog to the traditional mean-field formulation [11] because it decouples the Ω effect (mean toroidal flow) from the α effect (conversion of toroidal field into poloidal field from toroidal and poloidal flow fluctuations).

The transformation allows the simple two-vortex dynamo to be interpreted in terms of the same interactions of fluctuating flows and fluctuating magnetic fields that more complicated dynamo simulations achieve. The flow and field are broken up into

$$\begin{aligned} \mathbf{v} &= \overline{\mathbf{V}} + \widetilde{\mathbf{v}}, \\ \mathbf{B} &= \overline{\mathbf{B}} + \widetilde{\mathbf{b}}. \end{aligned} \tag{10}$$

Here an overbar denotes a mean value over the azimuth ($m = 0$) and a tilde denotes a fluctuating value ($m \neq 0$). The fluctuating components azimuthally average to zero, but they can beat together to generate a mean value

$$\begin{aligned} \overline{\widetilde{\mathbf{v}}} = \overline{\widetilde{\mathbf{b}}} = 0, \\ \overline{\widetilde{\mathbf{v}}\overline{\mathbf{B}}} = \overline{\widetilde{\mathbf{b}}\overline{\mathbf{V}}} = 0, \end{aligned}$$

but

$$\overline{\widetilde{\mathbf{v}}\widetilde{\mathbf{b}}} \neq 0.$$

It is useful to define a vector potential of the mean magnetic field $\overline{\mathbf{A}}$ such that

$$\begin{aligned} \overline{\mathbf{B}}(r,\theta) &= \nabla \times \overline{\mathbf{A}}(r,\theta), \\ \overline{\mathbf{A}}(r,\theta) &= \sum_{m_i=0} \nabla \times S_{\ell_i}^0(r) Y_{\ell_i}^0(\theta)\mathbf{e}_r + T_{\ell_i}^0(r) Y_{\ell_i}^0(\theta)\mathbf{e}_r \\ &= \sum_{m_i=0} -\frac{S_{\ell_i}^0}{r}\frac{\partial Y_{\ell_i}^0}{\partial \theta}\mathbf{e}_\phi + T_{\ell_i}^0 Y_{\ell_i}^0 \mathbf{e}_r. \end{aligned} \tag{11}$$

The reason for this is that the axisymmetric component of the magnetic field can be represented by two axisymmetric scalar functions

$$\overline{\mathbf{B}} = \overline{B_\phi}(r,\theta)\mathbf{e}_\phi + \nabla \times \overline{A_\phi}(r,\theta)\mathbf{e}_\phi. \tag{12}$$

Both of these scalar functions define divergence free vector fields

$$\nabla \cdot B_\phi \mathbf{e}_\phi = \nabla \cdot A_\phi \mathbf{e}_\phi = 0. \tag{13}$$

We can define a fluctuation driven emf

$$\mathcal{E}(r,\theta) \equiv \overline{\widetilde{\mathbf{v}} \times \widetilde{\mathbf{b}}} = \int_0^{2\pi} d\phi\, \widetilde{\mathbf{v}}(r,\theta,\phi) \times \widetilde{\mathbf{b}}(r,\theta,\phi) \tag{14}$$

and a mean-flow driven emf

$$\mathbf{E}(r,\theta) = \overline{\mathbf{V}}(r,\theta) \times (\overline{B_\phi}\mathbf{e}_\phi) + \overline{\mathbf{V}}(r,\theta) \times \nabla \times (\overline{A_\phi}\mathbf{e}_\phi) \tag{15}$$

and rewrite the magnetic induction equation (1) as time evolution equations for $\overline{A_\phi}$ and $\overline{B_\phi}$ coupled by these emfs:

$$\frac{\partial \overline{A_\phi}}{\partial \tau} = \mathcal{E} \cdot \mathbf{e}_\phi + \mathbf{E} \cdot \mathbf{e}_\phi + \nabla^2 \overline{A_\phi}, \tag{16}$$

$$\frac{\partial \overline{B_\phi}}{\partial \tau} = (\nabla \times \mathcal{E}) \cdot \mathbf{e}_\phi + (\nabla \times \mathbf{E}) \cdot \mathbf{e}_\phi + (\nabla^2 \overline{B_\phi}). \tag{17}$$

We note that $\nabla^2 \mathbf{B} = -\nabla \times \nabla \times \mathbf{B}$. Since we are looking at eigenvectors of the induction equation, the time derivative can be replaced by the eigenvalue. The emfs on the right-hand sides of Eqs. (16) and (17) can be treated as sources and sinks of the toroidal magnetic field and toroidal vector potential, respectively, by dotting each equation with $\overline{A_\phi}$ or $\overline{B_\phi}$ so that

$$\lambda \overline{A_\phi A_\phi} = \overline{A_\phi}\mathcal{E}_\phi + \overline{A_\phi}\mathbf{E}_\phi - \overline{A_\phi}(\nabla \times \overline{\mathbf{A}})_\phi, \tag{18}$$

$$\lambda \overline{B_\phi B_\phi} = \overline{B_\phi}(\nabla \times \mathcal{E})_\phi + \overline{B_\phi}(\nabla \times \mathbf{E})_\phi + \overline{B_\phi}\nabla^2 \overline{\mathbf{B}_\phi}. \tag{19}$$

These source and sink functions can be integrated over the sphere to give an indication of the total effect of each emf on the mean field

$$\langle \overline{A_\phi} e \rangle = \frac{\int_0^1 dr \int_0^\pi \sin(\theta) d\theta\, \overline{A_\phi}(r,\theta) e_\phi(r,\theta)}{\int_0^1 dr \int_0^\pi \sin(\theta) d\theta\, \overline{A_\phi}^2(r,\theta)}, \tag{20}$$

$$\langle \overline{B_\phi} e \rangle = \frac{\int_0^1 dr \int_0^\pi \sin(\theta) d\theta\, \overline{B_\phi}(r,\theta)(\nabla \times e)_\phi(r,\theta)}{\int_0^1 dr \int_0^\pi \sin(\theta) d\theta\, \overline{B_\phi}^2(r,\theta)}. \tag{21}$$

Here e is any of the emfs ($\mathcal{E}$, $\mathbf{E}$, $\nabla^2 \overline{A_\phi}$, or $\nabla^2 \overline{B_\phi}$). The the eigenvalue of the magnetic induction equation is the sum of all three emfs

$$\begin{aligned} \lambda &= \langle \overline{A_\phi}\mathcal{E} \rangle + \langle \overline{A_\phi}\mathbf{E} \rangle - \langle \overline{A_\phi}\nabla^2 \overline{A_\phi} \rangle \\ &= \langle \overline{B_\phi}\mathcal{E} \rangle + \langle \overline{B_\phi}\mathbf{E} \rangle - \langle \overline{B_\phi}\nabla^2 \overline{B_\phi} \rangle. \end{aligned}$$

IV. MEAN-FIELD EFFECTS AT LARGE AND SMALL SCALES

The mean-field theory definition of the fluctuation-driven emf posits that [11]

$$\mathcal{E} = \alpha \overline{\mathbf{B}} - \beta \nabla \times \overline{\mathbf{B}}. \tag{22}$$

Here α and β are functions of the statistical properties of the fluctuating flow and are defined as

$$\alpha = \frac{1}{3}\int_0^\infty d\tau\, \overline{\widetilde{\mathbf{v}}(\mathbf{r},t) \cdot \nabla \times \widetilde{\mathbf{v}}(\mathbf{r},t-\tau)}, \tag{23}$$

$$\beta = \frac{1}{3}\int_0^\infty d\tau\, \overline{\widetilde{\mathbf{v}}(\mathbf{r},t) \cdot \widetilde{\mathbf{v}}(\mathbf{r},t-\tau)}. \tag{24}$$

These functions are derived by assuming that the velocity fluctuations beat with the magnetic fluctuations that they induce from the mean field. The α effect drives a current parallel to the mean magnetic field and the β effect drives a current antiparallel to the curl of the magnetic field. In the large-eddy consideration the interaction of a poloidal velocity fluctuation with the magnetic fluctuation induced by the toroidal velocity fluctuation (and vice verse) is termed an

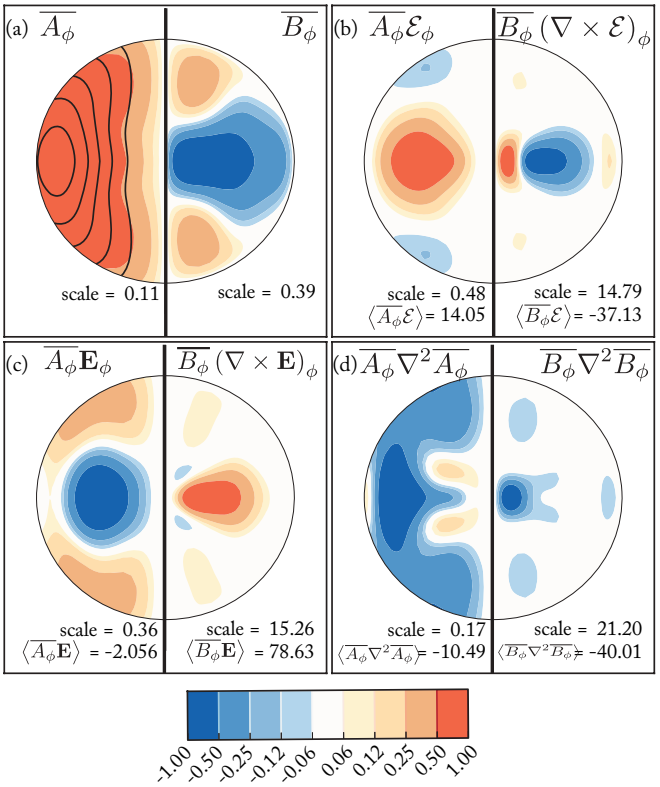

FIG. 4. (Color online) Toroidal vector potentials (left) and magnetic fields (right) in a Dudley-James two-vortex system. The color table is set to a logarithmic scale. Fields are calculated for Rm = 60, with an eigenvalue $\lambda = 1.49$. (a) Axisymmetric components of the fastest growing eigenmode at Rm = 60, with contours showing field lines of the poloidal magnetic field. (b) Fluctuation driven emfs [see Eq. (14)]. (c) Mean-flow driven emfs [Eq. (15)]. (d) Effect of diffusion upon the growing magnetic fields. The emfs are multiplied by the eigenmode so that orange (light) always indicates a strengthening of the local magnetic field and blue (dark) always indicates a weakening. The scaling for each plot is quoted at the bottom. For (b)–(d), $\langle\overline{A_\phi}e\rangle$ and $\langle\overline{B_\phi}e\rangle$ [see Eqs. (20) and (21)] are also quoted.

α effect. The relation to the mean field α becomes clear from the fact that the curl operation converts between toroidal and poloidal fields according to

$$\nabla\times\mathbf{v}=\sum_i \nabla\times\nabla\times t_i\mathbf{e}_r-\nabla\times\nabla^2 s_i\mathbf{e}_r. \qquad (25)$$

The toroidal and poloidal velocity fluctuations also interact with the magnetic fluctuations that they themselves induce. The relation to the mean field β effect is obvious.

Figure 4 represents the magnetic eigenmode [Fig. 4(a)] and the emfs that give rise to it in the spatial domain. The eigenmode is multiplied by the given emf so that orange (light) regions in Figs. 4(b)–4(d) indicate that energy is being transferred to the eigenmode via that portion of the emf. Blue (dark) regions indicate that energy is being removed from the eigenmode. The fluctuation-driven emf is shown [Fig. 4(b)] creating a mean poloidal field (left) while destroying a mean toroidal field (right). The creation of a poloidal field in a region where the toroidal field is being diminished suggests

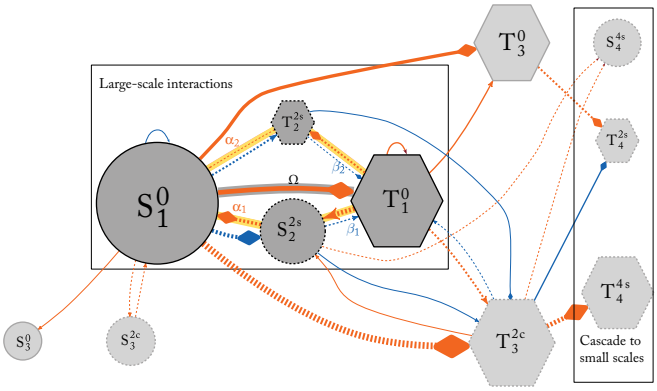

FIG. 5. (Color online) Network diagram representing the effect of the full Dudley-James $t2s2$ flow on a dynamo unstable eigenmode. The eigenmode represents Rm = 60, with an eigenvalue $\lambda = 1.49$. This network diagram follows the conventions of Fig. 3. The diagram is generated from the solution of the eigenvalue equation (7). The width of a given node is logarithmic in the amount of energy in that harmonic over the sphere $\langle B_k|B_k\rangle$ and the thickness of a given edge is linear in the coupling strength $\langle B_j|v_i|B_k\rangle$. The network is truncated at $\ell = 4$. Nodes with $\langle B_i|B_i\rangle$ less than 1.3% of $\langle S_1^0|S_1^0\rangle$ and interactions weaker than 10% of $\langle S_1^0|t_2^{2c}|T_3^{2c}\rangle$ are ignored. The α-Ω dynamo is highlighted and the β effect is labeled as in Fig. 3(b).

that the fluctuation-driven emf converts the toroidal magnetic field into a poloidal one. The toroidal field is then regenerated from the mean toroidal shear, which provides an Ω effect [Fig. 4(c)]. The mean poloidal flow sweeps the poloidal and toroidal fields out of the core of the sphere and out toward the edge, which reduces the effect of diffusion on destroying the magnetic field [Fig. 4(d)]. This last step is further explored in Sec. V.

We also construct a full network of spherical harmonic modes and interactions from the eigenmode and the flow matrix (Fig. 5) to better represent magnetic induction in terms of individual three-wave couplings. Like in Fig. 3, the nodes of the network represent the magnetic field harmonics and the edges represent valid interactions. However, now all of the couplings are apparent. Here the size of a given node is representative of how much energy is in that harmonic over the spherical domain $\langle B_k|B_k\rangle$ and the thickness of the edges represents how strong a given coupling $\langle B_j|v_i|B_k\rangle$ is. The box labeled "Large-scale interactions" is the full representation of the network shown previously in Fig. 3(b) calculated from the flow matrix and the eigenvector rather than just by the selection rules. The fundamental dynamic is still the mean toroidal flow generating an axisymmetric toroidal field from an axisymmetric dipole poloidal field (labeled Ω) and an α effect that converts the toroidal field back into the poloidal field while a β effect acts to diminish the toroidal field. The strongest coupling in the network is $\langle S_1^0|t_2^{2c}|T_3^{2c}\rangle$, but the effect of the T_3^{2c} harmonic on the primary dynamo cycle is small. Indeed, as is apparent from Fig. 5, all the higher-order magnetic fields cascade to smaller and smaller scales without great influence on the large-scale dynamics (thus the network is truncated at $\ell = 4$).

The advantage of this view is that it isolates the important couplings and interaction pathways more obviously than the

spatial view in Fig. 4. The relation between the spatial and spectral representations is that $\langle \overline{A_\phi}\mathbf{E}\rangle$ and $\langle \overline{B_\phi}\mathbf{E}\rangle$ represent the sum of all $\langle \overline{B}|\overline{v}|\overline{B}\rangle$ and $\langle \overline{A_\phi}\mathcal{E}\rangle$ and $\langle \overline{B_\phi}\mathcal{E}\rangle$ represent the sum of all $\langle \widetilde{B}|\widetilde{v}|\overline{B}\rangle$. Likewise, this is based on calculated couplings and is more physical than the schematic view presented in Fig. 3.

The network diagram justifies the appropriation of mean-field magnetohydrodynamics language. It confirms that the helical fluctuations are transferring energy from the toroidal field into the poloidal field, as was hinted by Fig. 4. The toroidal and poloidal fluctuating flows seed magnetic fluctuations from the mean toroidal field. The toroidal flow then beats with the magnetic fluctuation induced by the poloidal flow to generate a mean poloidal field (as per the α effect and labeled as such in the network). The toroidal and poloidal flow fluctuations also then beat with the magnetic fluctuations they themselves induce—$\langle T_1^0|t_2^{2s}|T_2^{2c}\rangle$ and $\langle T_1^0|s_2^{2s}|S_2^{2c}\rangle$, respectively—to remove energy from the mean toroidal field (as per the β effect and labeled as such in the network).

The cross sections (Fig. 4) and the network (Fig. 5) taken together demonstrate the dominance of large-scale dynamics in the evolution of the magnetic field. The axisymmetric component of the eigenmode is clearly dominated by the largest scales both radially (as evinced by the cross section) and spectrally (as evidenced by the amount of energy in the $\ell = 1$ modes). The network further confirms that the transfer of energy between poloidal and toroidal magnetic fields is dominated by the interactions of large-scale flows and large-scale fields.

V. EFFECTS OF FLOW PITCH AND MEAN FLOW COMPONENTS

Once a successful dynamo has been generated, it is possible to modify the flow to find the point where it no longer successfully dynamos. Dudley and James found a growing dynamo for only a single flow pitch ($\epsilon = 0.14$) of the set of pitches they tested at Rm $\leqslant 120$ ($\epsilon = 0.05, 0.10, 0.14, 0.20$). Figure 6 points to why this would be the case. The scan in the pitch angle reveals a bifurcation bubble, where two degenerate eigenvectors split such that one grows faster or decays slower than the other. The early studies of Dudley and James [15] bracket this bubble, with only a single pitch angle in the bubble. The range of dynamo unstable ϵ changes as a function of Rm, but has the fastest growth rate at $\epsilon \sim 0.13$.

Our analysis method allows us to study dynamo onset with specially constrained flows. Figure 7 shows the growth curves for flows with individual flow harmonics removed. Unsurprisingly, the loss of the Ω effect t_2^0 increases the dynamo threshold greatly. The dynamo can also still function when one fluctuation or the other (s_2^2 or t_2^2) is eliminated. At high enough Rm, other closed networks originating at S_1^0 generate more energy than is dissipated.

The flow with the highest $\mathrm{Rm_{crit}}$ is the one with the s_2^0 flow removed, despite the fact that this flow has a very weak signature in the network diagram of Fig. 5. The most readily apparent answer is that the s_2^0 flow adds advection to the system, which redistributes magnetic flux to mitigate the effects of diffusion. The signature is weak because the redistribution is neither a strong creator nor destroyer of total

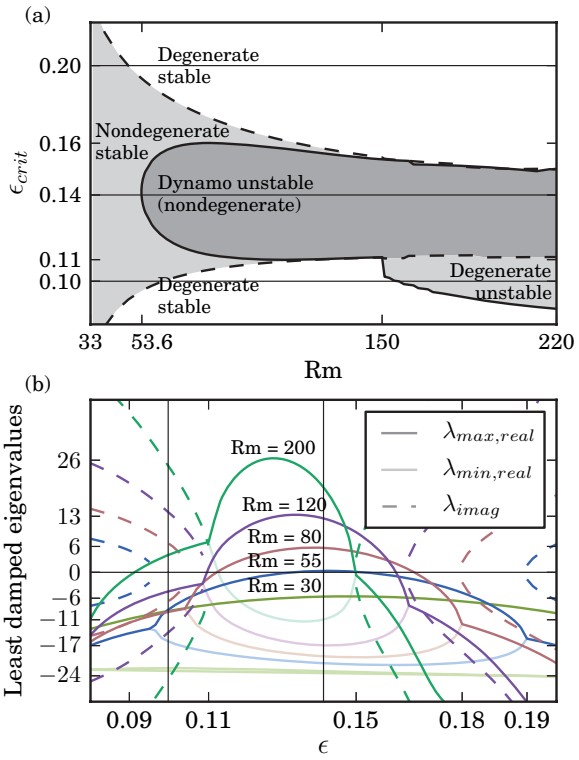

FIG. 6. (Color online) (a) Critical flow pitches plotted against Rm. (b) Largest eigenvalues plotted against ϵ at various Rm. The dashed lines in (a) represent the flow pitch in (b) where the real parts of the eigenvalues split. The thin black lines in each plot indicate the values of ϵ used by Dudley and James.

magnetic flux. To see this more clearly we examine the spatial distribution of emfs with no s_2^0 flow (Fig. 8). The dynamics of the poloidal field is relatively unchanged by the loss of poloidal advection. The eigenmode has the same general shape [left-hand sides of Figs. 4 and 8(a)]. The fluctuation-driven emf

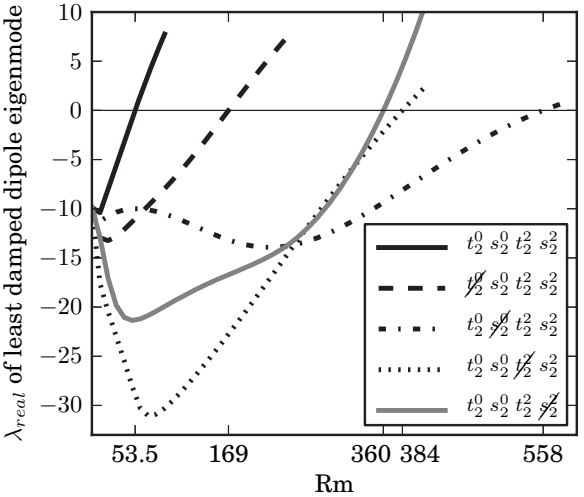

FIG. 7. Growth curves for the two-vortex flow with all flows (black solid line) and with individual flows removed. The $\mathrm{Rm_{crit}}$ are labeled on the x axis. The scans are performed with a resolution of 100 radial points and an $m_{\max} = \ell_{\max}$ of 7 and are likely significant to about 1% error (see the Appendix).

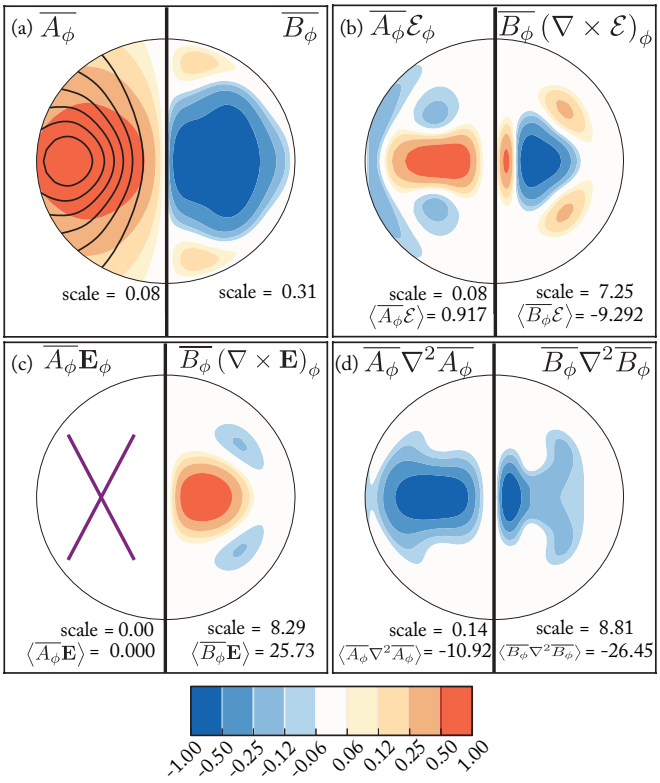

FIG. 8. (Color online) Toroidal vector potentials (left) and magnetic fields (right) in a Dudley-James two-vortex system with the s_2^0 flow eliminated. Fields are calculated for $\mathrm{Rm} = 60$, with an eigenvalue of $\lambda = -10.01$. The plots follow the same scheme as in Fig. 4. The left hemisphere of (c) is crossed out because there is no mean poloidal flow and the mean toroidal flow cannot drive a mean toroidal current.

$\mathcal{E}$ is weaker, but again has the same general shape [left hand sides of Figs. 4 and 8(b)]. The diffusion likewise has about the same effect [left-hand sides of Figs. 4 and 8(d)]. The toroidal field, however, suffers greatly from the loss of the poloidal advection. The shape of the field is similar [right-hand sides of Figs. 4 and 8(a)], but diffusion now completely matches the Ω effect [right-hand sides of Figs. 4 and 8(c) and 8(d)]. The turbulent emf continues to convert the toroidal magnetic field into a poloidal one, for a net loss of toroidal magnetic energy [Fig. 8(b)].

The reason for this dependence on poloidal advection is not obvious from the eigenmode calculation and its network of interactions presented here. The answer may be in an alternative formulation by Livermore and Jackson [21] where the growth of magnetic energy in the domain is the instability criterion (rather than the growth of individual eigenmodes, as studied here). They studied modified $t_1 s_2$ flows, similar to Dudley and James [15], and found that the poloidal advection is a necessary ingredient for instability and that small changes to the poloidal flow strongly affected the onset of the instability (and hence $\mathrm{Rm}_{\mathrm{crit}}$). Generally, the growth curve they found for a field with an S_1^0 component and $\mathrm{Rm} < 0$ was similar to the growth curve for a field with an S_1^1 component and $\mathrm{Rm} > 0$. This is consistent with our understanding from the coordinate transformation [Eq. (9)].

VI. CONCLUSION

The coordinate transformation presented in this paper has shown the simple and steady Dudley-James two-vortex dynamo to depend on effects from flows that are both coaxial with, and fluctuations relative to, the induced magnetic axis. This exposes the simple dynamo to more sophisticated analyses in terms that approximate those of mean-field theory. The usual terms of α, β, and Ω now have specific velocity components that they can attach to. Furthermore, the necessity of advection in countering diffusion to allow a large-scale magnetic field to grow is directly demonstrated by the difficulty of a dynamo without poloidal advection.

Much of the discussion of mean-field effects still focuses on scale-separated eddies [3,12], but there is numerical [13] and experimental [5] evidence that the large eddies are essential to understanding the conditions for dynamo onset. The work here shows that the large-eddy mean-field effects have been with us for a long time.

ACKNOWLEDGMENTS

The authors would like to acknowledge Dr. Mark Nornberg and Zane Taylor for useful discussions on the geometry of the two-vortex dynamo and Matt Elder for help in finding and using the graph layout software that built the coupling network diagrams (`Graphviz`). This work was supported by the Center for Magnetic Self-Organization in Laboratory and Astrophysical Plasmas.

APPENDIX A: DEFINITIONS AND NOMENCLATURE

The real, unnormalized spherical harmonics are defined as

$$Y_\ell^{m\left\{\begin{smallmatrix}c\\ s\end{smallmatrix}\right\}}(\theta,\phi) = P_\ell^m(\cos(\theta))\left\{\begin{smallmatrix}\cos(m\phi)\\ \sin(m\phi)\end{smallmatrix}\right\}, \tag{A1}$$

where P_ℓ^m is the associated Legendre polynomial. In this discussion we will denote the radial profile of a given harmonic according to

$$\langle B_j| \equiv B_j(r), \quad |B_k\rangle \equiv B_k(r),\ r \in [0,1]. \tag{A2}$$

We define an inner product as

$$\begin{aligned}\langle S_j|S_k'\rangle &= \delta_j^k N_k \int_0^1 dr \left(\frac{S_j(r)S_k'(r)\ell_k(\ell_k+1)}{r^2} + \frac{dS_j(r)}{dr}\frac{dS_k'(r)}{dr}\right),\\ \langle T_j|T_k'\rangle &= \delta_j^k N_k \int_0^1 dr\, T_j(r)T_k'(r),\\ N_i &= \frac{2\pi\left(1+\delta_{m_i}^0\right)\ell_i(\ell_i+1)}{2\ell_i+1}\frac{(\ell_i+m_i)!}{(\ell_i-m_i)!}.\end{aligned} \tag{A3}$$

The δ_j^k term is the Kroenecker delta and comes from the orthogonality of the poloidal and toroidal spherical harmonics. The energy of a single harmonic in the domain is given by $\langle B_i|B_i\rangle$.

In this notation, each individual flow harmonic is treated as an operator that converts one magnetic harmonic into others

using the relations of Eq. (A7),

$$\langle B_j|v_i = \sum_k (B_j \xrightarrow{v_i} B_k)\langle B_k|, \tag{A4}$$

i.e., the radial profile of a magnetic harmonic $\langle B_j|$ is being acted on by the flow harmonic v_i to generate several magnetic harmonics $\langle B_k|$. The strength of a coupling between two modes through a flow is characterized by $\langle B_j|v_i|B_k\rangle$. The orthogonality of harmonics means that the inner product will pick out only the projection onto the B_k mode. We draw our inspiration from the bra-ket notation of quantum mechanics, but we have modified the notation to fit more naturally with our notation of three-wave couplings.

The β effect can be represented in this notation as

$$\langle \overline{B_1}|\beta|\overline{B_1}\rangle = \langle \overline{B_1}|\widetilde{v_1}|\widetilde{B_i}\rangle\langle \widetilde{B_i}|\widetilde{v_1}|\overline{B_1}\rangle, \tag{A5}$$

while the α effect can be represented as

$$\langle \overline{B_1}|\alpha|\overline{B_2}\rangle = \langle \overline{B_1}|\widetilde{v_1}|\widetilde{B_i}\rangle\langle \widetilde{B_i}|\widetilde{v_2}|\overline{B_1}\rangle + \langle \overline{B_1}|\widetilde{v_2}|\widetilde{B_i}\rangle\langle \widetilde{B_i}|\widetilde{v_1}|\overline{B_1}\rangle. \tag{A6}$$

Here $\overline{B_{1,2}}$ are specific mean fields (B_1 and B_2 cannot both be S or T modes), $\widetilde{v_{1,2}}$ are specific fluctuating flows (which must have the same m order and again cannot both be s or t), and $\widetilde{B_i}$ may be either a single magnetic fluctuation or summed over all fluctuating modes. The interaction terms $B_j \xrightarrow{v_i} B_k$, where a source magnetic harmonic B_j is acted on by a flow harmonic v_i to create a magnetic harmonic B_k, are defined according to which of v_i, B_j, and B_k are poloidal and which are toroidal:

$$\begin{aligned}
(S_j \xrightarrow{s_i} S_k) &= \frac{K_{ijk}}{N_k}\left[p_i c_i s_i \frac{dS_j}{dr} - p_j c_j \frac{ds_i}{dr} S_j\right],\\
(S_j \xrightarrow{s_i} T_k) &= -\frac{L_{ijk}}{N_k}\left[p_j\left(\frac{d^2 s_i}{dr^2} - \frac{2}{r}\frac{ds_i}{dr}\right)S_j\right.\\
&\quad \left. -2\left(c_k \frac{ds_i}{dr} + \frac{p_i s_i}{r}\right)\frac{dS_j}{dr} + p_i s_i \frac{d^2 S_j}{dr^2}\right],\\
(T_j \xrightarrow{s_i} S_k) &= \frac{L_{ijk}}{N_k} p_i s_i T_j,\\
(T_j \xrightarrow{s_i} T_k) &= \frac{K_{ijk}}{N_k}\left\{\left[p_i c_i\left(\frac{ds_i}{dr} - \frac{2s_i}{r}\right) + p_k c_k \frac{ds_i}{dr}\right]T_j\right.\\
&\quad \left. + p_i c_i s_i \frac{dT_j}{dr}\right\},\\
(S_j \xrightarrow{t_i} S_k) &= \frac{L_{ijk}}{N_k} p_j t_i S_j,\\
(S_j \xrightarrow{t_i} T_k) &= -\frac{K_{ijk}}{N_k}\left[(p_k c_k + p_j c_j) t_i \frac{dS_j}{dr}\right.\\
&\quad \left. + p_j c_j\left(\frac{dt_i}{dr} - \frac{2t_i}{r}\right)S_j\right],\\
(T_j \xrightarrow{t_i} S_k) &= 0,\\
(T_i \xrightarrow{t_j} T_k) &= \frac{L_{ijk}}{N_k} p_k t_i T_j,
\end{aligned} \tag{A7}$$

where $p_i = \ell_i(\ell_i + 1)$.

TABLE I. Scan of eigenvalues of the $t2s2$ flow at Rm = 60 with respect to latitudinal and radial resolution. The memory capacity of the calculating computer limited the radial resolution scan to $\ell_{\max} = 10$. The bold numbers indicate the level of agreement with the $\ell_{\max} = 20$ case for rows 1–6 and the $n_r = 1600$ case for the last two rows.

$\ell_{\max}$	n_r	$\lambda(60)$	$\ell_{\max}$	n_r	$\lambda(60)$
9	100	**1.448**926	15	100	**1.456**606
10	100	**1.459**326	16	100	**1.456597**
11	100	**1.457**070	17	100	**1.456594**
12	100	**1.457**180	18	100	**1.456599**
13	100	**1.456**460	19	100	**1.456597**
14	100	**1.456**679	20	100	**1.456597**
10	200	**1.458**498	10	800	**1.458**241
10	400	**1.458**292	10	1600	**1.458**228

APPENDIX B: NETWORK GRAPHS AS A WAY OF UNDERSTANDING NONLINEAR INTERACTIONS

A long-standing problem in computer science is how to best lay out a graph to represent connections between different nodes in a network. A common algorithm is to create a network of springs, whose stiffness represents the strength of the connection between given nodes, and then find a minimum-energy configuration of nodes [22]. Programs that can automatically generate graph layouts are a common tool in exploratory data analysis. The graph of Fig. 5 was generated using one such tool, `Graphviz`, which is open source and maintained by AT&T Labs Research [23].

The kinematic dynamo problem is a good target for this kind of analysis because it is a linear problem; nodes and edges (couplings) are distinct from each other. All nodes are single magnetic harmonics. All edges represent the beating of a velocity harmonic with a magnetic harmonic to generate a second magnetic harmonic, the strength of a coupling between two modes is easy to calculate [see Eq. (A4)], and the selection rules of the Bullard-Gellman formalism [see Eqs. (3) and (4)] prevent the graph from becoming too cluttered. The graph layout highlights strong connections between magnetic

TABLE II. Comparison of eigenvalues of the $t2s2$ flow between axisymmetric flow and axisymmetric field calculations. These calculations were performed at Rm = 60 and scanned with respect to latitudinal and radial resolution. The calculations labeled "Axisymmetric field" were carried out with full azimuthal resolution ($m_{\max} = \ell_{\max}$). The bold numbers on the right half of the table indicate the agreement between the eigenvalues and the $\ell_{\max} = 20, n_r = 100$ case of Table I.

Axisymmetric flow			Axisymmetric field		
$\ell_{\max}$	n_r	$\lambda(60)$	$\ell_{\max}$	n_r	$\lambda(60)$
5	100	**1.**249179	5	100	**1.**249179
6	100	**1.**549141	6	100	**1.**549141
7	100	**1.491**581	7	100	**1.491**581
8	100	**1.**504970	8	100	**1.**504970
9	100	**1.448**926	9	100	**1.448**926
10	100	**1.459**326	10	100	**1.459**317
11	100	**1.457**070	11	100	**1.457**063
12	100	**1.457**180	12	100	**1.409**343

harmonics much more clearly than a tabular layout would by physically placing strongly coupled nodes near each other. As such, this is a good method for understanding complex three-wave interactions that are important in all turbulent systems.

APPENDIX C: THE PYNTDYN CODE

All of the numerical work in this paper was done using PYNTDYN, a kinematic dynamo simulation code based upon the work of Bullard and Gellman [19] and Dudley and James [15]. It uses the spherical harmonic expansion of the magnetic and velocity fields [Eq. (2)] and treats the radial functions S, T, s, and t with finite-difference methods. More advanced, spectral, codes have been developed with more favorable convergence properties [24], but the finite-difference solution is sufficient for the purpose of this work. Table I demonstrates the convergence properties of PYNTDYN solving the eigenvalue problem for a two-vortex flow.

`pyntdyn` is written in python, making heavy use of the `Numpy`, `Scipy`, and `Pysparsematrix` libraries. The eigenvalues and eigenvectors are found with Arnoldi iteration as implemented in ARPACK [25]. Table II demonstrates that the eigenvalue calculated under the rotation agrees with the unrotated eigenvalue to eight significant digits for $\ell_{\max} \leqslant 9$. The loss of agreement at higher resolutions is indicative of the cost of this transformation. The interaction terms in the advection matrix are proportional to $1/N$, as calculated in Eq. (A3). When nonaxisymmetric flows are included, a fully resolved calculation needs to include m in $[0, \ell_{\max}]$ rather than just $m = 1$ as in the axisymmetric flow case. Since N_i scales as $(\ell_i + m_i)!/(\ell_i - m_i)!$ [see Eq. (A3)], the larger $m_{\max}$ makes for an enormous N_i, which then spoils the condition number of the matrix.

[1] H. Moffatt, *Magnetic Field Generation in Electrically Conducting Fluids* (Cambridge University Press, Cambridge, 1978).

[2] A. S. Brun, M. S. Miesch, and J. Toomre, Astrophys. J. **614**, 1073 (2004).

[3] É. Racine, P. Charbonneau, M. Ghizaru, A. Bouchat, and P. K. Smolarkiewicz, Astrophys. J. **735**, 46 (2011).

[4] B. P. Brown, M. S. Miesch, M. K. Browning, A. S. Brun, and J. Toomre, Astrophys. J. **731**, 69 (2011).

[5] E. J. Kaplan, M. M. Clark, M. D. Nornberg, K. Rahbarnia, A. M. Rasmus, N. Z. Taylor, C. B. Forest, and E. J. Spence, Phys. Rev. Lett. **106**, 254502 (2011).

[6] F. Ravelet, M. Berhanu, R. Monchaux, S. Aumaître, A. Chiffaudel, F. Daviaud, B. Dubrulle, M. Bourgoin, P. Odier, N. Plihon, J.-F. Pinton, R. Volk, S. Fauve, N. Mordant, and F. Pétrélis, Phys. Rev. Lett. **101**, 074502 (2008).

[7] T. G. Cowling, Mon. Not. R. Astron. Soc. **94**, 39 (1933).

[8] J. E. P. Connerney, J. Geophys. Res. **98**, 18659 (1993).

[9] B. P. Brown, M. K. Browning, A. S. Brun, M. S. Miesch, and J. Toomre, Astrophys. J. **711**, 424 (2010).

[10] M. Ghizaru, P. Charbonneau, and P. K. Smolarkiewicz, Astrophys. J. Lett. **715**, L133 (2010).

[11] K. Krause and K. H. Rädler, *Mean Field Magnetohydrodynamics and Dynamo Theory* (Pergamon, New York, 1980).

[12] O. Gressel, D. Elstner, U. Ziegler, and G. Rüdiger, Astron. Astrophys. **486**, L35 (2008).

[13] B. Dubrulle, P. Blaineau, O. M. Lopes, F. Daviaud, J.-P. Laval, and R. Dolganov, New J. Phys. **9**, 308 (2007).

[14] M. Bourgoin, P. Odier, J.-F. Pinton, and Y. Ricard, Phys. Fluids **16**, 2529 (2004).

[15] M. L. Dudley and R. W. James, Proc. R. Soc. London Ser. A **425**, 407 (1989).

[16] K. Reuter, F. Jenko, and C. B. Forest, New J. Phys. **13**, 073019 (2011).

[17] R. Monchaux, M. Berhanu, M. Bourgoin, M. Moulin, P. Odier, J.-F. Pinton, R. Volk, S. Fauve, N. Mordant, F. Pétrélis, A. Chiffaudel, F. Daviaud, C. Gasquet, L. Marié, and F. Ravelet, Phys. Rev. Lett. **98**, 044502 (2007).

[18] J. Clyne and M. Rast, in *Visualization and Data Analysis 2005*, edited by R. F. Erbacher, J. C. Roberts, M. T. Grohn, and K. Borner, SPIE Proc. Vol. 5669 (SPIE, Bellingham, WA, 2005), pp. 284–294.

[19] E. Bullard and H. Gellman, Philos. Trans. R. Soc. London Ser. A **247**, 213 (1954).

[20] M. A. Blanco, M. Flórez, and M. Bermejo, J. Mol. Struct (THEOCHEM) **419**, 19 (1997).

[21] P. W. Livermore and A. Jackson, Proc. R. Soc. London Ser. A **460**, 1453 (2004).

[22] T. Kamada and S. Kawai, Inf. Process. Lett. **31**, 7 (1989).

[23] E. R. Gansner and S. C. North, Software: Practice Experience **30**, 1203 (2000).

[24] K. Li, P. W. Livermore, and A. Jackson, J. Comput. Phys. **229**, 8666 (2010).

[25] R. B. Lehoucq, D. C. Sorensen, and C. Yang, *Arpack Users' Guide: Solution of Large Scale Eigenvalue Problems by Implicitly Restarted Arnoldi Methods, 1997* (unpublished), URL [http://www.caam.rice.edu/software/ARPACK/].